Cell

Real-Time Observation of RecA Filament Dynamics with Single Monomer Resolution

Chirlmin Joo,[1] Sean A. McKinney,[1] Muneaki Nakamura,[2] Ivan Rasnik,[1,3] Sua Myong,[1] and Taekjip Ha[1,2,*]
[1] Howard Hughes Medical Institute and Department of Physics
[2] Department of Chemistry
University of Illinois at Urbana-Champaign, Urbana, IL 61801, USA
[3] Department of Physics, Emory University, Atlanta, GA 30322, USA
*Contact: tjha@uiuc.edu
DOI 10.1016/j.cell.2006.06.042

SUMMARY

RecA and its homologs help maintain genomic integrity through recombination. Using single-molecule fluorescence assays and hidden Markov modeling, we show the most direct evidence that a RecA filament grows and shrinks primarily one monomer at a time and only at the extremities. Both ends grow and shrink, contrary to expectation, but a higher binding rate at one end is responsible for directional filament growth. Quantitative rate determination also provides insights into how RecA might control DNA accessibility in vivo. We find that about five monomers are sufficient for filament nucleation. Although ordinarily single-stranded DNA binding protein (SSB) prevents filament nucleation, single RecA monomers can easily be added to an existing filament and displace SSB from DNA at the rate of filament extension. This supports the proposal for a passive role of RecA-loading machineries in SSB removal.

INTRODUCTION

RecA functions in homologous recombination, SOS response, and mutagenic DNA repair, which are essential for maintaining the integrity of genetic information (Cox, 1999; Kowalczykowski, 2000). A human homolog, Rad51, interacts with BRCA2, whose mutation increases susceptibility to breast and ovarian cancers (Venkitaraman, 2004). The copy number of RecA in *E. coli* is less than 10,000 in the basal level but increases by more than an order of magnitude during SOS response (Cox, 2003; Sommer et al., 1998); thus, the physiologically relevant concentration of RecA is in the micromolar range. The protein binds to single-stranded (ss) DNA to form a nucleoprotein filament that exhibits a helical structure (Story et al., 1992) with each pitch consisting of six RecA monomers and each monomer occupying approximately three nucleotides (nt) of the ssDNA (Egelman and Yu, 1989; Zlotnick et al., 1993). The ssDNA within the filament is stretched along the longitudinal axis of the filament and has the capability of seeking out and recognizing a double-stranded (ds) DNA of a homologous sequence to initiate a strand-exchange reaction during homologous recombination.

The formation of a RecA filament is highly cooperative and utilizes ATP as a cofactor (Menetski and Kowalczykowski, 1985). A number of monomers bind to ssDNA simultaneously during nucleation, but this crucial event is poorly understood because it has been difficult to separate nucleation from the subsequent filament extension that immediately follows. After nucleation, additional RecA units bind and extend the filament in the 3′ direction of the ssDNA. For this reason, we will refer to the 3′ end of ssDNA-RecA filament as the "3′-extending end." The unit of filament extension, whether it is the RecA monomer or higher-order complexes, is currently unknown for *E. coli* RecA. If the filament encounters an ss-dsDNA junction during extension, it continues to extend into the dsDNA (Register and Griffith, 1985). However, filament formation on dsDNA alone is extremely slow (Pugh and Cox, 1988) unless a 5′-ssDNA tail is present or the dsDNA is melted by applying strong force (Hegner et al., 1999) or torque (Fulconis et al., 2004). The rate of filament extension on dsDNA was determined by a single-molecule measurement (Shivashankar et al., 1999; van der Heijden et al., 2005), but the extension rate on ssDNA has been difficult to measure because of complications arising from multiple nucleation events.

RecA is a DNA-dependent ATPase and hydrolyzes ATP at the rate of 0.5 s^{-1} at 36°C (Bedale and Cox, 1996), regardless of where it is located on the filament (Brenner et al., 1987). When a monomer at the 5′ end of the filament, termed here "5′-disassembly end," hydrolyzes ATP, it dissociates from the filament (Lindsley and Cox, 1990; Register and Griffith, 1985) in a pH-dependent manner (Arenson et al., 1999). If RecOR interacts with the 5′-disassembly end (Shan et al., 1997), or if a slowly hydrolyzing ATP analog, ATPγS, is used, RecA dissociation becomes insignificant.

The difference between the two ends in terms of apparent stability may play a role during strand exchange via a treadmilling process, in which monomers dissociating from the 5′-disassembly end can rebind to the 3′-extending end so that a finite number of RecA monomers can be recycled efficiently and any discontinuity in the filament can be fixed (Menetski et al., 1990). A similar mechanism has been proposed for actin filaments, which show a large difference in dissociation constants between the two ends (Wegner, 1982). However, the rates with which RecA binds to the two ends and dissociates from the 3′-extending end are not known yet. Thus, the molecular mechanism for the directional growth of a RecA filament has not been clear.

In *E. coli*, most of a nascent ssDNA becomes occupied by SSB (ssDNA binding protein), preventing other proteins from accessing the ssDNA. Because of the highly cooperative nature of RecA binding, absence of a naked ssDNA precludes RecA-filament nucleation on SSB-coated ssDNA. Therefore, for RecA-mediated DNA repair to initiate on SSB-coated ssDNA, accessory proteins are necessary to help load RecA (Amundsen and Smith, 2003). Once RecA is loaded, SSB should no longer present a barrier to the 3′-extending end RecA filament (Kowalczykowski and Krupp, 1987; Thresher et al., 1988). To comprehend these two different modes of SSB function in relation to RecA, we need techniques that can observe the dynamic interactions between RecA and SSB in real time.

In the double-strand break repair (Cox et al., 2000; Kowalczykowski, 2000; Smith, 2001), a blunt-ended dsDNA is processed into a partial dsDNA with a 3′ tail, which becomes coated with SSB. After RecFOR occupies the ss-dsDNA junction (Morimatsu and Kowalczykowski, 2003), RecA displaces SSB assisted by RecOR (Bork et al., 2001; Umezu et al., 1993). How RecFOR helps load RecA on SSB-coated ssDNA is not yet clear. Likewise, RecA displaces SSB assisted by χ-modified RecBCD (Anderson and Kowalczykowski, 1997) and, in eukaryotes, Rad51 removes RPA supported by Brh2, a BRCA2 homolog (Yang et al., 2005).

Single-molecule FRET (Förster Resonance Energy Transfer) (Ha, 2001; Ha et al., 1996; Weiss, 1999) is a powerful method for observing the real-time dynamics of DNA (Lee et al., 2005; McKinney et al., 2005), RNA (Zhuang, 2005), protein-DNA interactions, and conformational changes of proteins (Diez et al., 2004; Myong et al., 2005). Here, we present single-molecule FRET assays that enabled us to watch binding and dissociation of individual RecA monomers in real-time. Combined with a novel analytic tool based on hidden Markov modeling, our work provides a new approach of determining not only the nature of the RecA binding and dissociation unit but also kinetic rates of the dynamics at both ends of the filament for the first time. Furthermore, by visualizing the dynamics of the filament near the ss-dsDNA junction, we provide insight into the role of RecA and its interactions with other proteins. In addition, we examine the filament nucleation process and determine its kinetic properties, as well as the minimum number of monomers required for nucleating a RecA filament. Finally, based on an assay in which a cluster of the filament is prenucleated near the ss-dsDNA junction, we find that RecA, once nucleated, is able to replace SSB almost as quickly as filament extension.

RESULTS

Single-Molecule FRET Assay

As illustrated in Figure 1A, a biotinylated dsDNA (18 base pairs) with a 3′-ssDNA tail is immobilized on a surface (Experimental Procedures). The donor (Cy3) and acceptor (Cy5) fluorophores are attached at the end of the ssDNA tail and the ss-dsDNA junction to report on changes in the end-to-end distance of the ssDNA through FRET. The ssDNA by itself is highly flexible (persistence length of ~1.5–3 nm), such that its conformational fluctuation is averaged out on a much faster time scale than our time resolution (Murphy et al., 2004). For the $(dT)_{21}$ tail, two dyes are in close proximity on average giving relatively high FRET efficiency, $E \sim 0.55$ (Figures 1A, left and 1Ca, white), in our standard solution condition (Experimental Procedures). Addition of 1 μM RecA and 1 mM ATPγS, our standard RecA and cofactor concentrations, leads to the filament formation and straightening of the ssDNA (Figure 1A, right). This results in low FRET, $E \sim 0.1$ (Figure 1Ca, green; different lengths of ssDNA in Figure S3B; different cofactors in Figure S4), distinguishable from acceptor blinking ($E = 0$) (Ha et al., 1999). Likewise, the DNA in-bulk solution shows high FRET without RecA and low FRET when the filament forms with ATPγS (Figure 1B).

Nucleation of a Filament

Whereas RecA forms a stable filament on the $(dT)_{21}$ tail with ATPγS, it does not form a filament stably when ATP is used as the cofactor; low FRET ($E \sim 0.1$) shows up only a small fraction of the time (6%) (Figure 1Cb). Likewise, the fluorescence spectrum in bulk does not show any significant change when RecA is added with ATP (Figure 1B). This observation confirms previous measurements, which found that RecA, together with ATP, does not form a stable filament on ssDNA lengths shorter than ~30 nt (Bianco and Weinstock, 1996; Brenner et al., 1987).

Examination of individual single-molecule traces reveals transient RecA binding, as evinced by occasional and brief transitions from high FRET ($E \sim 0.55$) to low ($E \sim 0.1$) (Figures 1D and S3C). Since the transient low-FRET state has an identical E value to that observed with the stable ATPγS-RecA filament (Figure 1Ca, green), we interpret it as representing brief formation of a RecA filament. While there must be several monomers in the filament formed on the $(dT)_{21}$ tail, the transitions between the two FRET states display only a few data points at 100 ms time resolution, much faster than expected from binding and dissociation of a monomer at an established filament (see Figure 2C; binding and dissociation of monomers take several seconds under the same condition). This was also true of $(dT)_{17}$ and $(dT)_{19}$. Therefore, there must be either simultaneous binding of multiple monomers or

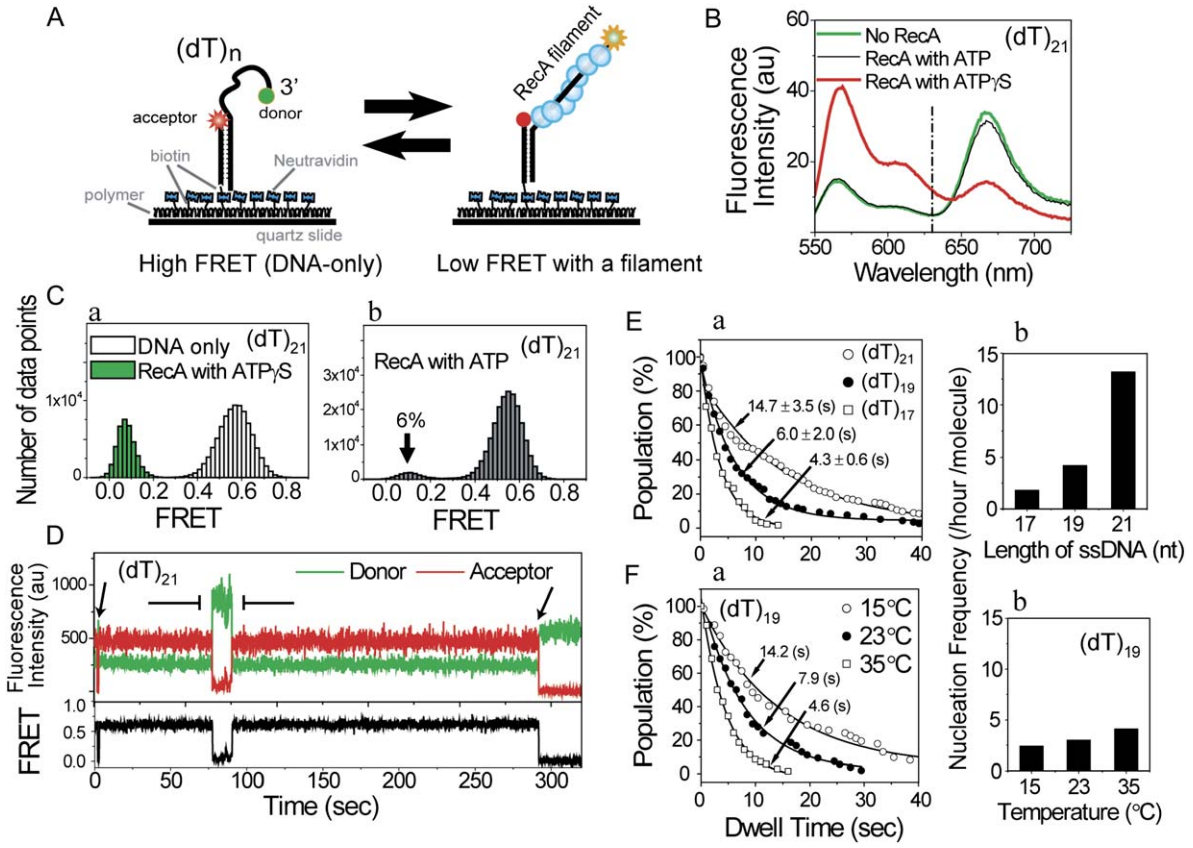

Figure 1. Filament Nucleation on Short ssDNA Tails

(A) A dsDNA with a 3′-$(dT)_n$ ssDNA tail is immobilized on a surface. FRET between fluorescent labels report on the changes in the average end-to-end distance of the ssDNA.

(B) Fluorescence spectra of $(dT)_{21}$ with (green) and without (red) RecA and ATPγS and with RecA and ATP (black) (after 10 min incubation).

(C) FRET histograms. (a) High FRET ($E \sim 0.55$) is from DNA only (white, 51 molecules) and low FRET ($E \sim 0.1$) is with RecA and ATPγS (green, 57 molecules, after 5 min incubation); (b) RecA with ATP ($E \sim 0.1$ and 0.55–114 molecules, after 5 min incubation). Data from donor-only molecules or periods were excluded.

(D) Time traces with RecA and ATP (100 ms time resolution). FRET efficiency stays high ($E \sim 0.55$) but briefly drops at t = 75 s. Acceptor blinking (left arrow) and photobleaching (right arrow) are distinguishable from the low FRET state.

(E) (a) Shown are normalized integrated dwell-time histograms for the low-FRET state versus ssDNA length (115, 119, and 228 events for 17, 19, and 21 nt) and exponential fits. Standard deviations (SDs) are from three data sets. (b) Shown are resulting nucleation frequency (602, 614, and 350 molecules from left).

(F) (a) Shown are normalized integrated dwell-time histograms for the low-FRET state at different temperatures with $(dT)_{19}$ (62, 54, and 70 events for 15°C, 23°C, and 35°C). (b) Also shown is nucleation frequency (479, 212, and 344 molecules from left).

binding of a preassembled oligomer in order for RecA to form a cluster of a filament on such short ssDNA.

We then determined the average dwell time of the low-FRET state with different lengths of ssDNA tail and found that shorter ssDNA yields a shorter average dwell time (Figure 1Ea). Meanwhile, the average dwell time decreases as the temperature increases (Figure 1Fa), and this is inversely proportional to the increase in the ATP hydrolysis rate (Bedale and Cox, 1996). These dependences suggest that the stability of the cluster is correlated with the number of monomers bound to ssDNA and ATP hydrolysis. Next, we measured how frequently the cluster forms. The frequency sharply drops when shorter lengths of ssDNA than $(dT)_{21}$ are used (Figure 1Eb). Furthermore, there is no filament formation observed with $(dT)_{13}$ and $(dT)_{15}$. Finally, the frequency of cluster formation depends only weakly on the temperature (Figure 1Fb). These collective findings suggest that the transition observed here represents the formation/dissociation of a nucleation cluster that would likely lead to filament extension on a longer ssDNA.

Dynamics at the 5′-Disassembly End

For an ssDNA longer than ~30 nt, a RecA filament forms stably even with ATP. In this case, FRET changes would reflect the assembly/disassembly occurring at the ends

of the filament rather than the formation/dissociation of the nucleation cluster. Since FRET between the two ends of such a long naked ssDNA is relatively low, we sought to achieve high resolving power in FRET by placing the donor internally on the ssDNA tail without disrupting DNA backbone or perturbing RecA activity (Figure 2A; Supplemental Experimental Procedures; further discussion in the Supplemental Data). The ssDNA of $(dT)_{13+46}$ has the donor and acceptor separated by 13 nt, followed by 46 nt of 3′ tail so that FRET changes reflect the dynamics at the 5′-disassembly end. This DNA shows high FRET ($E \sim 0.65$) by itself but exhibits low FRET ($E \sim 0.15$) in the presence of RecA and ATPγS (Figure 2Ba) due to stable filament formation.

In contrast, a broad FRET histogram spanning from 0.15 to 0.7 is observed with RecA and ATP (Figure 2Bb). Examining the single-molecule traces, we find that they exhibit stepping between well-defined FRET levels (Figure 2C). Traces no longer exhibit the simple two-state dynamics found in shorter tails, suggesting that different binding modes (i.e., different numbers of RecA monomers on the 13 nt region between donor and acceptor) are being observed. If these different FRET values correspond to different assembly states of the filament, we may expect to see up to five different FRET values (0, 1, 2, 3, and 4 monomers) because up to four monomers could bind to the 13 nt region. However, not only is it challenging to identify five states given the limited signal-to-noise ratio, but it could also bias the analysis to presume that there exist five states. Therefore, we employed a newly developed form of hidden Markov modeling (HMM) to analyze the data statistically without imposing a preconceived model (See Experimental Procedures) (McKinney et al., 2006). HMM analysis identifies distinct FRET states in each trace (Figure 2C, the fit in green) and determines the number of states, their FRET values, and the transition rates between them (Figure 2D).

Figure 2Da shows the result of HMM analysis as a transition density plot (TDP) of 17,203 transitions from 165 DNA molecules. A TDP is effectively a two-dimensional histogram that shows how frequent transitions are between different states. They are presented with the FRET levels prior to and after the transition on the horizontal and vertical axes respectively. It is evident that there are four distinct FRET values (0.15, 0.3, 0.5, and 0.7) along each axis, in addition to the no-FRET peaks due to acceptor blinking. The highest FRET value ($E \sim 0.7$) agrees with the DNA-only value (Figure 2Ba, green), therefore the state with $E \sim 0.7$ is designated M_0. The lowest FRET value ($E \sim 0.15$) is close to the value observed with RecA and ATPγS (Figure 2Ba, white). Thus, the remaining FRET values ($E \sim 0.5$, 0.3, and 0.15) are termed M_1, M_2, and M_3, respectively, with each number representing the number of monomers bound contiguously, starting from the donor location to the 13 nt segment (Figure 2A). Noncontiguous binding of RecA was not considered because we did not detect any binding of RecA to $(dT)_{13}$ with ATP (see the previous section); de novo nucleation of a filament in such a short ssDNA segment is extremely unlikely, and the binding transitions here represent extension from the existing filament only.

It is not clear why only three monomers appear to bind instead of four. When we shortened the ssDNA segment between the donor and acceptor using $(dT)_{5+54}$ and $(dT)_{10+49}$, we observed that transitions occur primarily between two and three states, indicating that one and two monomers can access the 5 and 10 nt segments respectively (TDP in Figure 2F and time traces in Figure S5). The TDP in Figures 2D and 2F show that the most frequent transitions are of the type $M_i \rightarrow M_{i\pm1}$, indicating that the majority, >78% for $(dT)_{13+46}$ and >93% for $(dT)_{10+49}$, of binding and dissociation events occurs one monomer at a time. Note that the mirror symmetry in the TDPs comes from the fact that the majority of transitions are of the type $M_i \rightarrow M_{i\pm1}$ and that the system under observation is in equilibrium, when the number of transitions of $M_i \rightarrow M_{i+1}$ is the same as that of $M_{i+1} \rightarrow M_i$.

Once every transition in the plot is classified according to which $M_i \rightarrow M_j$ pair it belongs to, kinetic rates can be determined for each pair (Figure 2Db). For example, the binding rates ($k_{on(obs)}^{M0\rightarrow M1}$, $k_{on(obs)}^{M1\rightarrow M2}$, and $k_{on(obs)}^{M2\rightarrow M3}$) can be determined as a function of RecA concentration (Figure 2Ea). As expected, all $k_{on(obs)}$'s increase with increasing RecA concentration. We also find $k_{on(obs)}^{M0\rightarrow M1} > k_{on(obs)}^{M1\rightarrow M2} > k_{on(obs)}^{M2\rightarrow M3}$ at the following two highest different RecA concentrations: 1 μM and 0.25 μM. This effect may be due to the reduction in the amount of naked ssDNA available for binding as the number of bound monomers increases.

The dissociation rates ($k_{off}^{M1\rightarrow M0}$, $k_{off}^{M2\rightarrow M1}$, and $k_{off}^{M3\rightarrow M2}$) are largely independent of RecA concentration, as one would expect (Figure 2Eb), but vary slightly with the position at the two highest RecA concentrations, 1 μM and 0.25 μM. We should point out that the average k_{off} (averaged over all three dissociation rates) is not necessarily equal to or lower than the ATPase rate (k_{cat}). In fact, it was shown that when a monomer leaves the 5′-disassembly end, k_{off} of the adjacent monomer is twice k_{cat} (Arenson et al., 1999). Thus, such an effect should be considered when M_i has been arrived at via RecA dissociation. When the probability for M_i to have come about via RecA dissociation is p and the coupling efficiency of ATP hydrolysis to dissociation is φ,

$$k_{off} = \varphi \times (2k_{cat} \times p + k_{cat} \times [1 - p]): \qquad \text{Equation (1)}$$

Then, from p and k_{off} values determined by HMM analysis and TDP (Figure 2Db), we can calculate the "corrected" dissociation rate ($k^*_{off} = \varphi \times k_{cat}$) (Figure S6A). This rate of 0.12 ± 0.02 (s^{-1}), independent of the position of the dissociating monomer and RecA concentration, is comparable to the ATPase rate of 0.18 s^{-1} at 22°C, estimated from Bedale and Cox by extrapolation (Bedale and Cox, 1996). This comparison indicates that the coupling efficiency φ is close to 1 in accord with the previous estimate at neutral pH (Arenson et al., 1999). Finally, the value of k^*_{off} is similar to $k_{on(obs)}$, 0.11 ± 0.02 (s^{-1}) in the presence of 100 nM

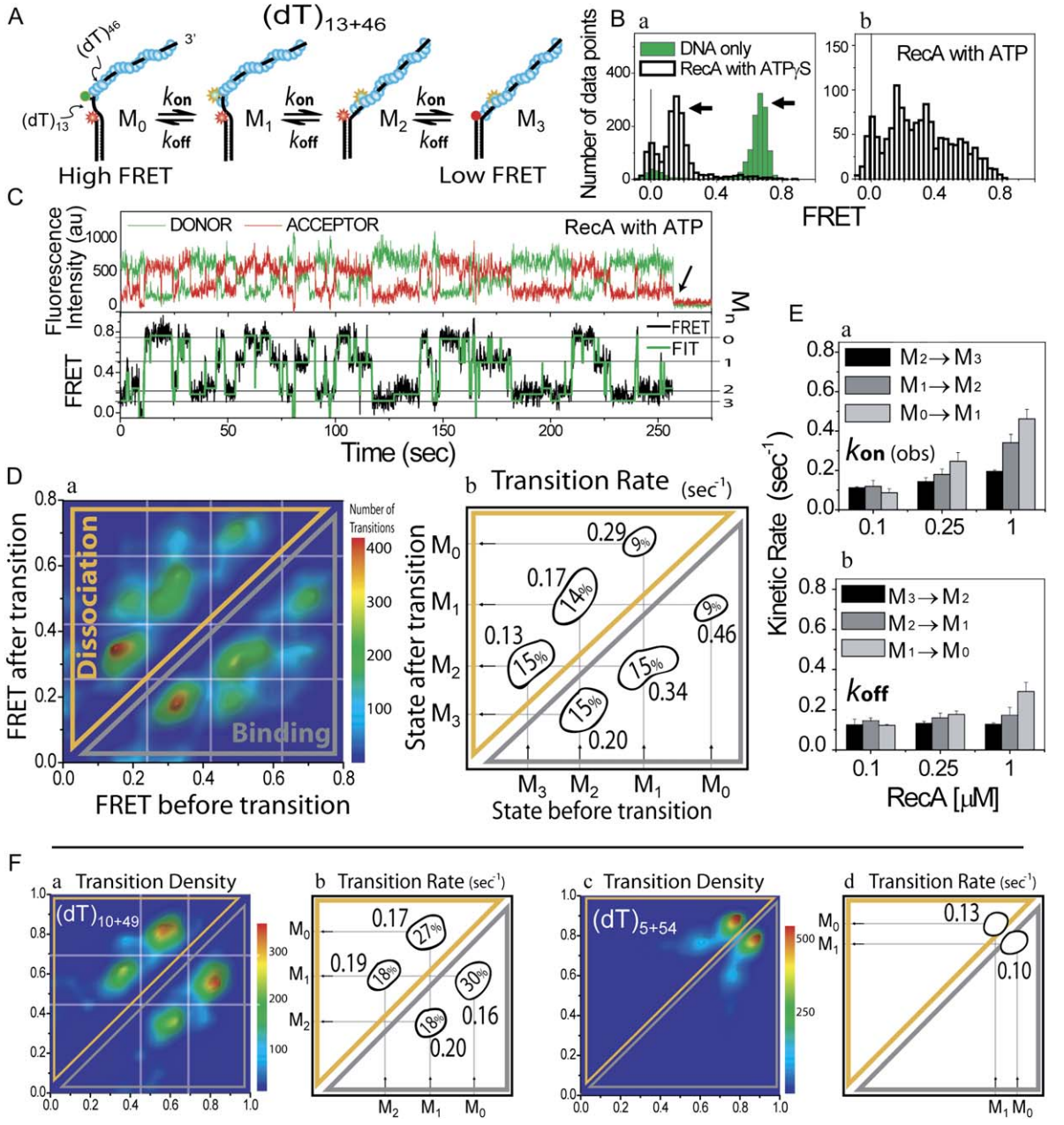

Figure 2. Dynamics at the 5′-Disassembly End

(A) FRET reports on the dynamics at the 5′-disassembly end.

(B) FRET histograms (a) from DNA only ($E \sim 0.65$, green) and with RecA and ATPγS ($E \sim 0.15$, white, after 2 min incubation) and (b) with RecA and ATP (after 30 min incubation). Vertical gray lines mark $E = 0$ due to donor-only species.

(C) Time traces with RecA and ATP (100 ms time resolution). The FRET trace (black) is fitted by HMM (green); then, four states are assigned (M_0, M_1, M_2, and M_3, based on the TDP in [Da]). Donor photobleaching was at $t \sim 255$ s (arrow).

(D) Transition density plot (TDP). (a) This pseudo-3D plot is constructed by adding a Gaussian peak for each transition. There are four states with $E \sim 0.15$, 0.3, 0.5, and 0.7. (b) Rates and frequencies (inside circles) of each transition, $M_i \rightarrow M_{i\pm1}$, are presented in the same scheme.

(E) (a) Binding and (b) dissociation rates versus RecA concentration for different transitions (based on 12,204 transitions from 172 molecules at 0.1 μM, 23,580 from 196 at 0.25 μM, and 17,203 from 165 at 1 μM). The errors are SDs of three datasets each.

(F) TDP and kinetic rates (a and b) with $(dT)_{10+49}$ tail based on 8637 transitions from 104 molecules ($E \sim 0.35$, 0.6 and 0.8) (c and d) and with $(dT)_{5+54}$ based on 5917 transitions from 92 molecules ($E \sim 0.8$ and 0.9).

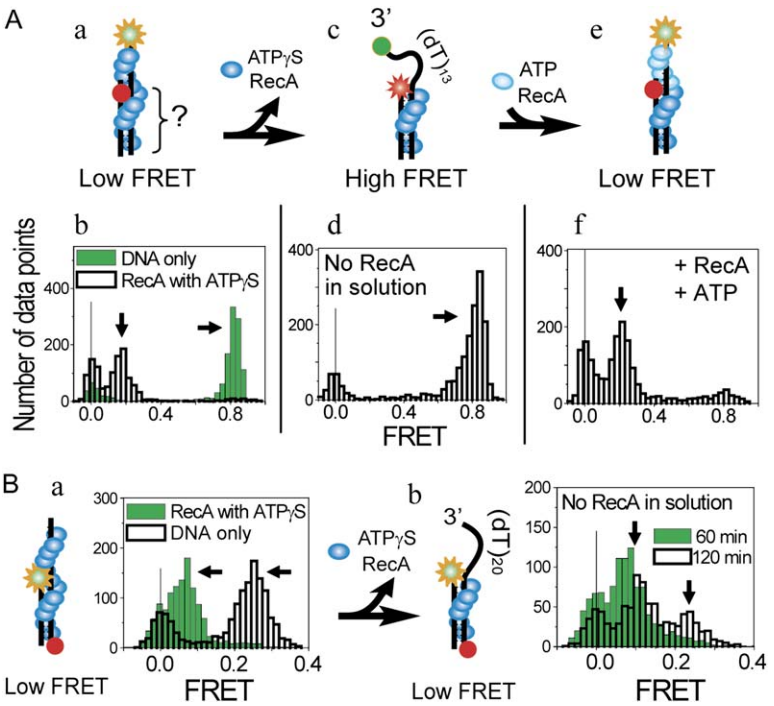

Figure 3. Stable Formation of <dsDNA|ATPγS> as a Nucleation Cluster

(A) (a and b) Filament formation on a 3′-$(dT)_{13}$ tail of a partial dsDNA shows lower FRET ($E \sim 0.2$, white, after 20 min incubation) than DNA only ($E \sim 0.8$, green). (c and d) <ssDNA|ATPγS> disassembles in ~5 min upon RecA and ATPγS removal from solution, and FRET is restored to the DNA-only value ($E \sim 0.8$, after 10 min incubation). (e and f) When RecA and ATP are added, stable <ssDNA|ATP> forms quickly, assisted by <dsDNA|ATPγS>, and FRET returns to a low value ($E \sim 0.2$, after <1 min incubation).

(B) (a) Filament formation on the dsDNA of a partial dsDNA results in $E \sim 0.1$ (green, 15 min incubation) compared to $E \sim 0.25$ of DNA only (white). (b) <dsDNA|ATPγS> does not disassemble up to 1 hr after removal of RecA and ATPγS but does slowly afterwards.

RecA, so we estimate that the dissociation constant (K_D) is about 100 nM at the 5′-disassembly end.

Filament Formation with ATPγS

Next, we attempted to observe the filament dynamics at the 3′-extending end using a ssDNA tail of $(dT)_{46+13}$, the same DNA as $(dT)_{13+46}$ but labeled differently so that FRET reports on the dynamics of the 13 nt segment at the 3′-extending end. At 1 μM RecA, this DNA gave stable low FRET, indicating filament formation with no discernible dynamics at the 3′-extending end (data not shown). At 100 nM, we observed irregular FRET fluctuations, likely as a result of both formation/dissociation of the nucleation cluster and the assembly/disassembly at the 3′-extending end (data not shown), precluding detailed analysis. We realized that what we needed was a method to separate the nucleation step from the filament extension. We could achieve just that, based on an unexpected finding that we will discuss in this section.

As described earlier, stable filaments form on short ssDNA tails, from $(dT)_{13}$ to $(dT)_{21}$ (Figure 1Ca) if ATPγS is used as a cofactor (Leahy and Radding, 1986). Here, we will refer to such filament as <ssDNA|ATPγS>. With $(dT)_{13}$, <ssDNA|ATPγS> results in low FRET ($E \sim 0.2$) (Figure 3Ab, white). If RecA is subsequently removed from solution via flow while keeping the magnesium concentration constant (Figures 3Ac and 3Ad), the single-molecule FRET histogram is restored to that of DNA only within 5 min (Figure 3Ab, white), indicating that the ssDNA tail becomes free of RecA. Single-molecule traces recorded during this disassembly reveal individual states (M_i) of $(dT)_{13}$ (Figure S8). While the disassembly was also observed with $(dT)_{15}$–$(dT)_{21}$ tails (data not shown), longer tails, $(dT)_{40}$ and $(dT)_{70}$, however, supported stable <ssDNA|ATPγS> even after removing free RecA and ATPγS (data not shown) and required SSB for RecA removal from ssDNA (Figure 5B).

To study a possible filament formation of <dsDNA|ATPγS>, we attached the donor and acceptor fluorophores at the ends of dsDNA, which has a 3′ tail of $(dT)_{20}$ (Figure 3Ba). E decreases from 0.25 to 0.1 when RecA and ATPγS are added, indicating the formation of <dsDNA|ATPγS>. Since it cannot form in the absence of an ssDNA tail (Figure S9C), its formation here must be through extension of <ssDNA|ATPγS> into dsDNA (Shaner et al., 1987; Shaner and Radding, 1987). Furthermore, by utilizing a different configuration of labeling (Figure S9A) and by a footprinting assay (Figure S9B), we found that the filament forms over the entire length of dsDNA.

Next, when RecA and ATPγS are removed from solution, no significant change in FRET is observed for 1 hr, while it slowly starts to disassemble in 2 hr (Figure 3Bb), suggesting unexpectedly high stability of <dsDNA|ATPγS> (>1 hr) compared to <ssDNA|ATPγS> formed on 13–21 nt ssDNA (<5 min). A similar property was observed at high temperature (35°C) (Figure S10B) and also with dsDNA that has 5′-ssDNA tail (Figure S11).

Dynamics at the 3′-Extending End

The difference in stability between <ssDNA|ATPγS> and <dsDNA|ATPγS> in the absence of free RecA results in a unique configuration in which a filament is present only around the dsDNA portion of a partial duplex DNA (Figure 3Ac). We suspected that the <dsDNA|ATPγS> in such

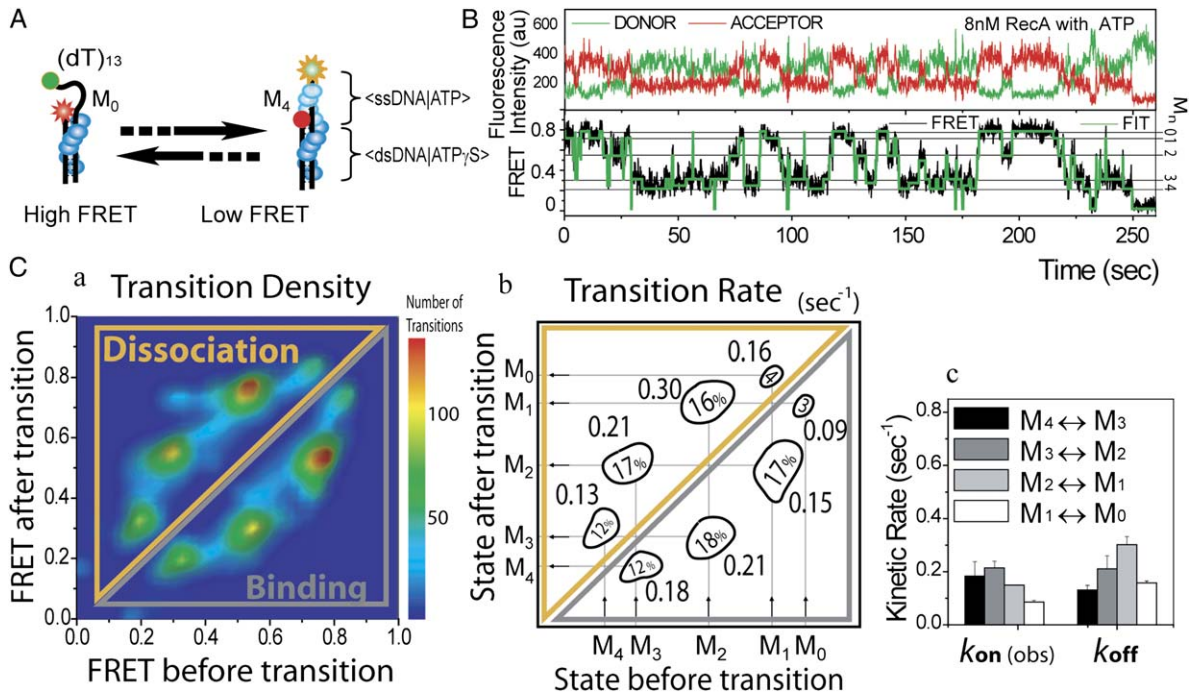

Figure 4. Dynamics at the 3′-Extending End

(A) FRET reports on the dynamics at the 3′-extending end. The stable <dsDNA|ATPγS> facilitates the formation of <ssDNA|ATP>.

(B) Time traces with ATP and 8 nM RecA (100 ms time resolution).

(C) (a) TDP shows five FRET states ($E \sim 0.2$, 0.3, 0.55, 0.75, and 0.85) based on 4635 transitions from 82 molecules. (b and c) The binding and dissociation rates and frequencies (inside circles) of each transition are shown. The errors are the SDs from two datasets each.

a construct might act as a nucleation cluster, thus facilitating the formation of <ssDNA|ATP> when RecA is added with ATP. Indeed, we observe stable filament formation on $(dT)_{13}$ within 1 s of adding RecA and ATP (Figures 3Ae and 3Af), whereas there was no or rare filament formation observed with 13–21 nt ssDNA without <dsDNA|ATPγS> (Figure 1Eb). The similar observation was made also at a higher temperature (35°C) (Figure S10A). This unexpected finding allows us to decouple filament extension from nucleation and enables the observation of filament dynamics at very low RecA concentrations.

Figure 4B shows FRET fluctuations after the addition of 8 nM RecA with ATP, indicative of filament dynamics at the 3′-extending end (Figure 4A). Transitions between multiple FRET states detected in single-molecule time traces are presented in the TDP (Figure 4Ca; 82 molecules and 4635 transitions), where five different states are clearly discerned ($E \sim 0.2$, 0.3, 0.55, 0.75, and 0.85; M_4, M_3, M_2, M_1, and M_0, respectively), consistent with the maximum number of states counted in Figure S8Ba. Almost all transitions occur between the nearest neighbors, $M_i \leftrightarrow M_{i\pm1}$, again suggesting that the unit of binding and dissociation is a monomer also for the 3′-extending end. It also provides the most direct evidence thus far that RecA cannot dissociate from the middle of the filament.

$k_{on(obs)}^{M0\rightarrow M1}$ is significantly lower than those at other positions (Figure 4Cc, left). Excluding $k_{on(obs)}^{M0\rightarrow M1}$, the average $k_{on(obs)}$ is 0.18 ± 0.03 s^{-1}. $k_{off}^{M2\rightarrow M1}$, $k_{off}^{M3\rightarrow M2}$, and $k_{off}^{M4\rightarrow M3}$ vary with respect to one another but the corrected dissociation rates are nearly identical with the exception of $k^*_{off}{}^{M1\rightarrow M0}$ (Figure S6B). There appears to be a high-energy barrier between M_0 and M_1, that slows both binding and dissociation, probably due to the junction of heterofilaments, <ssDNA|ATP> and <dsDNA|ATPγS> (Prevost and Takahashi, 2003). The average k^*_{off} (excluding $k^*_{off}{}^{M1\rightarrow M0}$) of 0.16 ± 0.04 ($s^{-1}$) is close to the average $k_{on(obs)}$ in the presence of 8 nM RecA; thus, K_D must be about 8 nM in the 3′-extending end.

RecA Displaces SSB Easily when Supported by a Preformed Nucleation Cluster at an ss-dsDNA Junction

The binding of an SSB tetramer to the 3′ $(dT)_{70}$ ssDNA tail of a partial dsDNA, a structure that would be produced in the double-strand break repair, results in high FRET ($E \sim 0.7$) in our solution condition (Figure 5A). This is likely caused by the wrapping of ssDNA around SSB, observed both in crystallography and ensemble FRET studies (Kozlov and Lohman, 2002; Raghunathan et al., 2000). In comparison, FRET is very low in the absence of any protein ($E \sim 0.1$) and in the presence of RecA ($E \sim 0$) (Figures 5Ab and 5Bc). Once SSB binds to the ssDNA, it does not come off appreciably even after 1 hr in the absence of free SSB in solution (data not shown). Upon addition of RecA

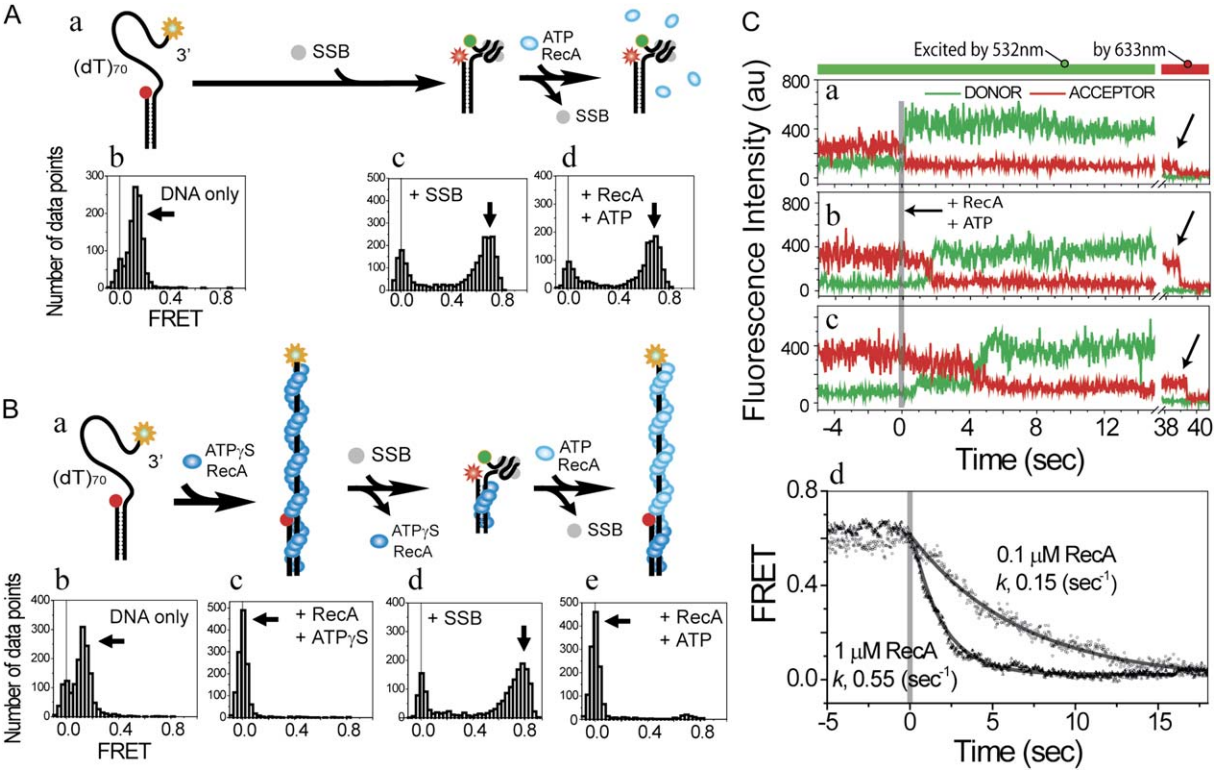

Figure 5. RecA Displaces SSB Bound to $(dT)_{70}$ Only when Supported by a Preformed Nucleation Cluster

(A) (a) Shown is the inability of RecA to displace SSB bound to $(dT)_{70}$. (b) Also shown is a FRET histogram with DNA only ($E \sim 0.1$). (c) With 10 nM SSB, DNA wraps around the protein ($E \sim 0.7$, after 5 min incubation). (d) When RecA and ATP are added, replacing SSB in solution, there is no change observed in FRET ($E \sim 0.7$, after 1 hr incubation).

(B) (a) RecA displaces SSB efficiently, given a preformed nucleation cluster. (b) Shown is a FRET histogram with DNA only ($E \sim 0.1$). (c) A RecA filament forms around the dsDNA as well as the ssDNA ($E \sim 0$, after 15 min incubation). (d) After adding 10 nM SSB and removing RecA and ATPγS, <ssDNA|ATPγS> is effectively removed by the binding of SSB ($E \sim 0.7$, after 15 min incubation). (d) When RecA and ATP are added, replacing SSB in solution, RecA quickly forms a filament, displacing SSB efficiently ($E \sim 0$, after <1 min incubation).

(C) Time traces show the transitions from the SSB bound form ($E \sim 0.7$) to the RecA filament ($E \sim 0$) (30 ms time resolution). After solution exchange (t = 0), E drops through diverse pathways: FRET changes (a) without any intermediate state and (b) with one or (c) more intermediate state(s) were found with comparable frequencies. To distinguish the low FRET ($E \sim 0$) from fluorescence signal with an inactive acceptor, the activity of the acceptor was checked by directly exciting the acceptor using a 633 nm laser at t > 38 s (arrows). (d) A group of FRET traces (57 molecules for 1 μM RecA; 26 for 0.1 μM) are averaged and fitted by exponential decay curves.

and ATP, SSB remains even after 1 hr (Figure 5Ad), indicating that SSB is extremely difficult to be displaced by RecA.

We wondered whether RecA might form a filament by replacing SSB if <dsDNA|ATPγS>, the preassembled nucleation cluster at the junction, is present. As illustrated in Figure 5B, adding RecA and ATPγS to the partial dsDNA results in very low FRET (Figure 5Bc). If we then add 10 nM SSB but remove RecA and ATPγS from solution, SSB slowly binds to ssDNA by disassembly of <ssDNA|ATPγS> (Figure 5Bd), eventually returning to the single-molecule FRET histogram identical to what was obtained with SSB alone (Figure 5Ac) with a time scale of ~5 min (Figure S13), suggesting that SSB has replaced the RecA filament on the ssDNA. Strikingly, upon subsequent addition of RecA and ATP, the FRET peak shifts to a very low FRET within seconds (Figure 5Be), indicating efficient formation of a stable filament. Such rapid filament formation is in sharp contrast to the data obtained without the preassembled nucleation cluster (Figure 5Ad), where RecA and ATP could not displace SSB during a 1 hr observation window.

The detailed process by which RecA replaces SSB is shown in single-molecule time traces (Figures 5Ca–5Cc). After the solution containing RecA and ATP is flowed in to replace the SSB solution at t = 0, FRET efficiency drops largely monotonically via diverse pathways, with a rate of 0.55 s^{-1} (Figure 5Cd). This replacement is almost as fast as the RecA-filament formation on a bare ssDNA facilitated by <dsDNA|ATPγS> (k = 0.8 s^{-1}; Figure S12), implying that SSB is displaced with little resistance by a 3′-extending end of the filament.

DISCUSSION

In this work, we have established new single-molecule FRET assays capable of observing binding and dissociation of individual RecA monomers in the nucleoprotein filament. The kinetic rates of the filament dynamics have been determined via a novel analysis based on the hidden Markov model. Below, we summarize the most important conclusions that can be drawn from our studies.

The Minimum Size of the Nucleation Cluster

A RecA-nucleation cluster forms briefly and infrequently on 17–21 nt-long ssDNA. The actual processes of formation and dissociation of the cluster were faster than we could resolve clearly with the time resolution of 100 ms. The dwell time of the cluster formed on 17 and 19 nt tails were 4.3 and 6.0 s, respectively (Figure 1Ea), similar to the dissociation time of a single RecA monomer $(k^*_{off})^{-1}$, 8.3 s. This coincidence implies that dissociation of even a single monomer makes the cluster bound to 17–19 nt very unstable and induces rapid dissociation of the cluster. Furthermore, the nucleation frequency dropped precipitously when the ssDNA length was below 21 nt (Figure 1Eb), and no nucleation was observed with 13 and 15 nt. Therefore, ~5 monomers bound to 17 nt could be considered the minimum unit for nucleation.

The Unit of Binding and Dissociation

Since free *E. coli* RecA exists in solution in diverse assembly states, including a monomer, trimer, hexamer, and so on (Brenner et al., 1990), there has been no definitive way to determine the size of a binding unit in the filament assembly. Because the filament binding and dissociation transitions occurred predominantly between nearest neighbor states, as revealed in the TDPs (Figures 2D, 2F, and 4C), we conclude that this unit of binding as well as of dissociation is primarily a single monomer. The data further indicate that dissociation occurs from the extremities of the filament because extensive dissociation from the internal sites on the filament would have yielded a much more significant amount of nonnearest neighbor transitions.

Binding Rates at Each End

The individual monomer binding rates $k_{on(obs)}$ have been directly measured at both 3′-extending and 5′-disassembly ends. In previous works, binding of RecA to the 5′-disassembly end had been largely ignored in describing the dynamics of a filament, but we found that the $k_{on(obs)}$ was even higher than k_{off} at the 5′-disassembly end at 1 μM RecA. The RecA filament was thought to exhibit a monotonic disassembly followed by a rapid recovering assembly in a previous analysis, which neglected RecA binding at the 5′-disassembly end (Tlusty et al., 2004), but we observed continual binding and dissociation of monomers (Figure 2C). Thus, RecA binding at the 5′-disassembly end should be included in the description of filament dynamics.

We also determined the heretofore immeasurable $k_{on(obs)}$ at the 3′-extending end (0.18 s^{-1} at 8 nM RecA). As a rudimentary comparison, if we extrapolate to 1 μM, $k_{on(obs)}$ becomes 23 s^{-1}, which coincides with the rate determined with dsDNA (20 s^{-1} in the same RecA concentration [van der Heijden et al., 2005]).

Dissociation Rates at Either End

The dissociation rates k_{off} were also measured at both ends. k_{off} at the 5′-disassembly end was consistent with the previous report (Arenson et al., 1999), and k_{off} at the 3′-extending end was determined for the first time. k_{off} at the 5′-disassembly end and at the 3′-extending end were essentially the same. Meanwhile, there is about an order of magnitude difference in the dissociation constant of ~100 nM at the 5′-disassembly end and ~8 nM at the 3′-extending end. Therefore, the directionality in the filament growth is mainly due to the difference in the binding rates.

The dissociation rate after correction (k^*_{off}) was close to the ATPase rate, showing that disassembly of a filament is tightly coupled with ATPase activity. k^*_{off} was independent of the position of the dissociating monomer, indicating that there is no significant coupling between neighbor monomers in terms of ATPase activity (Shan et al., 1996).

RecA Replaces SSB if Given a Nucleation Site

It has been long known that RecA can displace SSB from ssDNA (Kowalczykowski and Krupp, 1987). Using a preassembled nucleation cluster, here we provided the most comprehensive evidence that SSB is removed by an extending RecA filament. The rates of SSB removal and the unhindered extension rate of the RecA filament were found to be almost identical, suggesting that the hindrance provided by SSB to a growing filament is minimal. Even though an unraveled section of ssDNA between the nucleation cluster and SSB must be very small, RecA could still bind and extend the filament with ease. Therefore, how SSB can function in two contrasting modes in relation to RecA is clearly explained; the ssDNA binding energy of SSB is smaller than that of the RecA filament so that SSB can be easily removed by an extending filament, but the exposed length in SSB-saturated ssDNA is shorter than ~17 nt, such that a de novo nucleation of a filament is inhibited.

Our result supports the proposal that a sufficient role for the RecA-loading machineries in helping RecA replace SSB is to provide a nucleation cluster-like structure to initiate RecA-filament extension (Anderson and Kowalczykowski, 1997). If so, no active SSB-clearing mechanism is required for the RecA-loading machineries (Kowalczykowski, 2005). Crystallography revealed that the interface between BRCA2 and Rad51 bears a clear resemblance to the interface between neighbor Rad51 monomers in Rad51 filaments (Conway et al., 2004; Pellegrini et al., 2002). It is possible that the RecA-loading machineries, RecBCD (Spies and Kowalczykowski, 2006) and RecFOR, might have adopted the same strategy by emulating the

surface of the filament that free RecA monomers in solution easily access and bind to.

RecA Filament near the Junction

There were no dissociation events observed from <ssDNA|ATP> when its 5′-disassembly end was stabilized by <dsDNA|ATPγS> at 1 μM RecA, analogous to the stabilization of the 5′-disassembly end by RecOR (Shan et al., 1997). We therefore expect that once a RecA filament forms assisted by RecA-loading proteins, other proteins would not be able to access the ssDNA or the junction (Figure 6B).

In the absence of such stabilizing factors, for example, after the RecA-loading proteins have left the junction, a stretch of ssDNA next to the junction would become exposed due to the intrinsic instability of the 5′-disassembly end (Figures 6C and 6D). Since the FRET histogram of $(dT)_{13+46}$ was broadly biased toward low FRET at 1 μM RecA (Figure 2Bb), the exposed ssDNA is shorter than ~13 nt on average. Stronger bias toward low FRET was observed with a longer segment between donor and acceptor as expected (Figure S7). When RecA concentration was lowered to 0.1 μM, the histogram of $(dT)_{13+46}$ shifted toward high FRET (data not shown), indicating that more than 13 nt is routinely exposed.

Our data therefore show that ssDNA accessibility at the junction of a 3′-tailed dsDNA is modulated by RecA concentration. When the RecA concentration is above ~1 μM, the filament would not be immediately destroyed but would go through constant fluctuations of limited range (Figure 6C). Therefore, RecA would still retain to a large extent the capacity to perform its role, the degree of which would be higher than previously thought since the binding at the 5′-disassembly end is significant. On the contrary, at submicromolar concentrations, the filament would disassemble swiftly (Figure 6D). Indeed, we found that the activity of Rep helicase that unwinds 3′-tailed dsDNA was affected by RecA concentration and that SSB binding to ssDNA was greatly delayed by the presence of 1 μM RecA in solution (unpublished data).

RecA Filament In Vivo

Based on our findings, we propose the following scenarios of protein interactions during the first steps of the double-strand break repair (Figure 6). When a blunt-ended dsDNA is processed into a partial dsDNA, SSB binds to the 3′ ssDNA tail generated. Then, the RecA-loading machinery binds to the junction and recruits and holds RecA (Anderson and Kowalczykowski, 1997; Bork et al., 2001; Kowalczykowski, 2005; Morimatsu and Kowalczykowski, 2003; Pellegrini et al., 2002; Spies and Kowalczykowski, 2006; Umezu et al., 1993; Yang et al., 2005), nucleating a RecA filament. Additional RecA monomers bind successively to extend the filament in the 3′ direction, displacing SSB (Kowalczykowski and Krupp, 1987; Thresher et al., 1988). The filament is very stable not only because the 5′-disassembly end is held by the RecA-loading machinery (Shan et al., 1997) but also because the K_D of the 3′-extending end is much lower than the concentration of RecA in the basal level. Therefore, neither the ssDNA tail nor the junction is easily accessible for binding by other proteins. The 5′-disassembly end becomes unstable if the RecA-loading machinery leaves the junction, but because the basal level of RecA is still higher than the K_D of the 5′-disassembly end, only a small region of ssDNA near the junction becomes accessible to other proteins. Future experiments, including the RecA-loading machineries, may test these ideas directly.

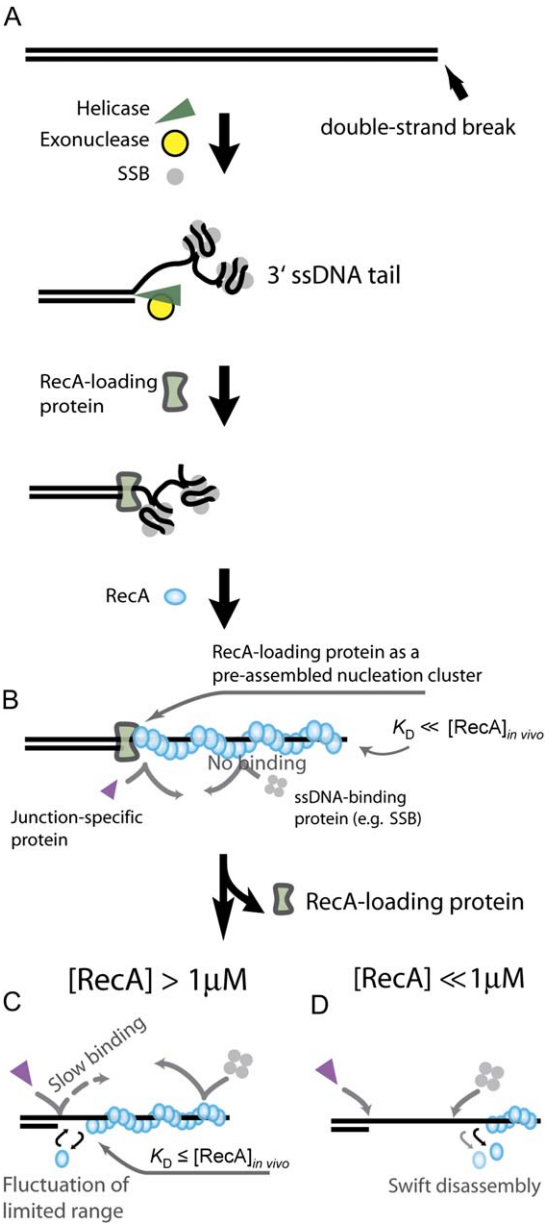

Figure 6. Model for Assembly of the RecA Filament and Its Stability In Vivo

EXPERIMENTAL PROCEDURES

Reaction Condition for Single-Molecule Assay

As shown in Figure S1, DNA is immobilized on a quartz surface (Finkenbeiner), which is coated with polyethyleneglycol (a method in the Supplemental Experimental Procedures) in order to eliminate nonspecific surface adsorption of proteins (Ha et al., 2002). The immobilization was mediated by biotin-Neutravidin binding between biotinylated DNA (IDTDNA), Neutravidin (Pierce), and biotinylated polymer (PEG-MW 5,000, Nektar Therapeutics). About 100 pM of DNA molecules are immobilized and observed in our standard solution condition: 1 mM ATP (Sigma) or ATPγS (Calbiochem), 10 mM MgAc, 100 mM NaAc, 25 mM Tris-Ac at pH 7.5 in the presence of oxygen scavenging system of 1 mg/ml glucose oxidase (Sigma), 0.4% $(w/v)_D$-glucose (Sigma), 0.04 mg/ml catalase (Roche), and 1% v/v 2-mercaptoethanol (Acros) at room temperature (22 ± 1°C) unless otherwise specified. The concentration of RecA (New England Biolabs) is 1 μM unless otherwise specified. SSB (10 nM, the standard concentration) (a gift from Dr. T.M. Lohman) was not added unless mentioned. A prepared solution ~100 μl was injected into an assembled chamber that holds ~20 μl. Therefore, the injection results in a very efficient change in chemical environments around immobilized DNA. When RecA and ATP are in the injected solution, the system inside the chamber reaches equilibrium in less than a minute.

Single-Molecule Data Acquisition

Cy3 on DNA is excited by an Nd:YAG laser (532 nm, 75 mW, CrystaLaser) via total internal reflection (Figure S1). The fluorescence signal from Cy3 and Cy5 that is collected by a water immersion objective lens (60×, Olympus) goes through a 550 nm long-pass filter to block out laser scattering. It is separated by a 630 nm dichroic mirror and is detected by EMCCD camera (Andor) with a time resolution of 30–200 ms. Fluorescence signal of donor and acceptor molecules is amplified before camera readout; therefore, the recorded fluorescence intensity is in an arbitrary unit. The signal was recorded using software written in Visual C++. Single-molecule traces were extracted from the recorded video file by IDL software.

Single-Molecule Data Analysis

Basic data analysis on the single-molecule traces were carried out by Origin and software written in Matlab, with which FRET efficiency, E, is calculated as "acceptor intensity" divided by the sum of "donor and acceptor intensities" after correcting for the crosstalk between the donor and acceptor signals, ~15%.

Single-molecule FRET histograms in Figures 2, 3, and 5 are from more than 1000 molecules from multiple imaging areas. The width of individual peaks in the histograms is typically about 0.1 (full width at half maximum) and is mainly due to statistical and instrumental noise. The standard error is typically less than 0.01. $E = 0$ peak in FRET histograms (marked by vertical lines) is due to "donor-only" molecules for which the acceptor is not present or inactive.

The complex single-molecule traces arising from RecA binding and dissociation were analyzed by hidden Markov modeling, which is more reliable, reproducible, and less susceptible to human bias than traditional thresholding algorithms (McKinney et al., 2006). Recognizing that our system can be recast as a hidden Markov model, we used an optimizing Viterbi algorithm to determine the most likely combination of FRET states, noise, and transition rates for each trace. Though a certain number of distinct FRET values were expected, given our system, we did not impose it in our analysis. Instead, the algorithm was asked to find more than the number of expected states (for example, twice) and to determine those states' noise (assumed to be a Gaussian sigma), their state-to-state transition probabilities, and the number of each transition type occurring in that trace. To speed up analysis, the Turing CPU cluster was used.

Supplemental Data

Supplemental Data include thirteen figures and experimental procedures and can be found with this article online at http://www.cell.com/cgi/content/full/126/3/515/DC1/.

ACKNOWLEDGMENTS

We wish to thank Jiajie Diao, Salman Syed, Mary C. McKinney, Benjamin C. Stevens, Sungchul Hohng, Michelle K. Nahas, Burak Okumus, S. MacLaren, and C. Lei for experimental help; Rahul Roy, Jin Yu, Ibrahim Cisse, Jeehae Park, Kaushik M. Ragunathan, and Dr. Michael M. Cox (University of Wisconsin at Madison) for helpful discussion; Dr. Timothy M. Lohman (Washington University) and his lab for providing DNA and proteins; and the Laboratory of Fluorescence Dynamics for letting us share their facilities. We gratefully acknowledge computer time provided by the UIUC on the Turing Xserve Cluster for data analysis. Funds for research were provided by NSF (Grants PHY-0134916 and DBI-0215869), by NIH (Grant GM065367), and by Cottrell Scholarship Awards. S.A.M. is an NSF graduate research fellow.

Received: February 1, 2006
Revised: May 16, 2006
Accepted: June 20, 2006
Published: August 10, 2006

REFERENCES

Amundsen, S.K., and Smith, G.R. (2003). Interchangeable parts of the Escherichia coli recombination machinery. Cell *112*, 741–744.

Anderson, D.G., and Kowalczykowski, S.C. (1997). The translocating RecBCD enzyme stimulates recombination by directing RecA protein onto ssDNA in a chi-regulated manner. Cell *90*, 77–86.

Arenson, T.A., Tsodikov, O.V., and Cox, M.M. (1999). Quantitative analysis of the kinetics of end-dependent disassembly of RecA filaments from ssDNA. J. Mol. Biol. *288*, 391–401.

Bedale, W.A., and Cox, M. (1996). Evidence for the coupling of ATP hydrolysis to the final (extension) phase of RecA protein-mediated DNA strand exchange. J. Biol. Chem. *271*, 5725–5732.

Bianco, P.R., and Weinstock, G.M. (1996). Interaction of the RecA protein of Escherichia coli with single-stranded oligodeoxyribonucleotides. Nucleic Acids Res. *24*, 4933–4939.

Bork, J.M., Cox, M.M., and Inman, R.B. (2001). The RecOR proteins modulate RecA protein function at 5′ ends of single-stranded DNA. EMBO J. *20*, 7313–7322.

Brenner, S.L., Mitchell, R.S., Morrical, S.W., Neuendorf, S.K., Schutte, B.C., and Cox, M.M. (1987). recA protein-promoted ATP hydrolysis occurs throughout recA nucleoprotein filaments. J. Biol. Chem. *262*, 4011–4016.

Brenner, S.L., Zlotnick, A., and Stafford, W.F. (1990). RecA protein self-assembly.2. analytical equilibrium ultracentrifugation studies of the entropy-driven self-association of RecA. J. Mol. Biol. *216*, 949–964.

Conway, A.B., Lynch, T.W., Zhang, Y., Fortin, G.S., Fung, C.W., Symington, L.S., and Rice, P.A. (2004). Crystal structure of a Rad51 filament. Nat. Struct. Mol. Biol. *11*, 791–796.

Cox, M.M. (1999). Recombinational DNA repair in bacteria and the RecA protein. Prog. Nucleic Acid Res. Mol. Biol. *63*, 311–366.

Cox, M.M. (2003). The bacterial RecA protein as a motor protein. Annu. Rev. Microbiol. *57*, 551–577.

Cox, M.M., Goodman, M.F., Kreuzer, K.N., Sherratt, D.J., Sandler, S.J., and Marians, K.J. (2000). The importance of repairing stalled replication forks. Nature *404*, 37–41.

Diez, M., Zimmermann, B., Borsch, M., Konig, M., Schweinberger, E., Steigmiller, S., Reuter, R., Felekyan, S., Kudryavtsev, V., Seidel, C.A.,

and Graber, P. (2004). Proton-powered subunit rotation in single membrane-bound F0F1-ATP synthase. Nat. Struct. Mol. Biol. *11*, 135–141.

Egelman, E.H., and Yu, X. (1989). The location of DNA in RecA-DNA helical filaments. Science *245*, 404–407.

Fulconis, R., Bancaud, A., Allemand, J.F., Croquette, V., Dutreix, M., and Viovy, J.L. (2004). Twisting and untwisting a single DNA molecule covered by RecA protein. Biophys. J. *87*, 2552–2563.

Ha, T. (2001). Single-molecule fluorescence methods for the study of nucleic acids. Curr. Opin. Struct. Biol. *11*, 287–292.

Ha, T., Enderle, T., Ogletree, D.F., Chemla, D.S., Selvin, P.R., and Weiss, S. (1996). Probing the interaction between two single molecules: fluorescence resonance energy transfer between a single donor and a single acceptor. Proc. Natl. Acad. Sci. USA *93*, 6264–6268.

Ha, T.J., Ting, A.Y., Liang, J., Deniz, A.A., Chemla, D.S., Schultz, P.G., and Weiss, S. (1999). Temporal fluctuations of fluorescence resonance energy transfer between two dyes conjugated to a single protein. Chem. Phys. *247*, 107–118.

Ha, T., Rasnik, I., Cheng, W., Babcock, H.P., Gauss, G.H., Lohman, T.M., and Chu, S. (2002). Initiation and re-initiation of DNA unwinding by the Escherichia coli Rep helicase. Nature *419*, 638–641.

Hegner, M., Smith, S.B., and Bustamante, C. (1999). Polymerization and mechanical properties of single RecA-DNA filaments. Proc. Natl. Acad. Sci. USA *96*, 10109–10114.

Kowalczykowski, S.C. (2000). Initiation of genetic recombination and recombination-dependent replication. Trends Biochem. Sci. *25*, 156–165.

Kowalczykowski, S.C. (2005). Cancer: catalyst of a catalyst. Nature *433*, 591–592.

Kowalczykowski, S.C., and Krupp, R.A. (1987). Effects of Escherichia coli SSB protein on the single-stranded DNA-dependent ATPase activity of Escherichia coli RecA protein. Evidence that SSB protein facilitates the binding of RecA protein to regions of secondary structure within single-stranded DNA. J. Mol. Biol. *193*, 97–113.

Kozlov, A.G., and Lohman, T.M. (2002). Stopped-flow studies of the kinetics of single-stranded DNA binding and wrapping around the Escherichia coli SSB tetramer. Biochemistry *41*, 6032–6044.

Leahy, M.C., and Radding, C.M. (1986). Topography of the interaction of recA protein with single-stranded deoxyoligonucleotides. J. Biol. Chem. *261*, 6954–6960.

Lee, J.Y., Okumus, B., Kim, D.S., and Ha, T. (2005). Extreme conformational diversity in human telomeric DNA. Proc. Natl. Acad. Sci. USA. *102*, 18938–18943.

Lindsley, J.E., and Cox, M.M. (1990). Assembly and disassembly of RecA protein filaments occur at opposite filament ends. Relationship to DNA strand exchange. J. Biol. Chem. *265*, 9043–9054.

McKinney, S.A., Freeman, A.D., Lilley, D.M., and Ha, T. (2005). Observing spontaneous branch migration of Holliday junctions one step at a time. Proc. Natl. Acad. Sci. USA *102*, 5715–5720.

McKinney, S.A., Joo, C., and Ha, T. (2006). Analysis of single molecule FRET trajectories using hidden Markov modeling. Biophys. J. *91*, 1941–1951.

Menetski, J.P., and Kowalczykowski, S.C. (1985). Interaction of Reca protein with single-stranded-DNA - quantitative aspects of binding-affinity modulation by nucleotide cofactors. J. Mol. Biol. *181*, 281–295.

Menetski, J.P., Bear, D.G., and Kowalczykowski, S.C. (1990). Stable DNA heteroduplex formation catalyzed by the Escherichia coli RecA protein in the absence of ATP hydrolysis. Proc. Natl. Acad. Sci. USA *87*, 21–25.

Morimatsu, K., and Kowalczykowski, S.C. (2003). RecFOR proteins load RecA protein onto gapped DNA to accelerate DNA strand exchange: a universal step of recombinational repair. Mol. Cell *11*, 1337–1347.

Murphy, M.C., Rasnik, I., Cheng, W., Lohman, T.M., and Ha, T. (2004). Probing single-stranded DNA conformational flexibility using fluorescence spectroscopy. Biophys. J. *86*, 2530–2537.

Myong, S., Rasnik, I., Joo, C., Lohman, T.M., and Ha, T. (2005). Repetitive shuttling of a motor protein on DNA. Nature *437*, 1321–1325.

Pellegrini, L., Yu, D.S., Lo, T., Anand, S., Lee, M., Blundell, T.L., and Venkitaraman, A.R. (2002). Insights into DNA recombination from the structure of a RAD51-BRCA2 complex. Nature *420*, 287–293.

Prevost, C., and Takahashi, M. (2003). Geometry of the DNA strands within the RecA nucleofilament: role in homologous recombination. Q. Rev. Biophys. *36*, 429–453.

Pugh, B.F., and Cox, M.M. (1988). General mechanism for RecA protein binding to duplex DNA. J. Mol. Biol. *203*, 479–493.

Raghunathan, S., Kozlov, A.G., Lohman, T.M., and Waksman, G. (2000). Structure of the DNA binding domain of E. coli SSB bound to ssDNA. Nat. Struct. Biol. *7*, 648–652.

Register, J.C., 3rd, and Griffith, J. (1985). The direction of RecA protein assembly onto single strand DNA is the same as the direction of strand assimilation during strand exchange. J. Biol. Chem. *260*, 12308–12312.

Shan, Q., Cox, M.M., and Inman, R.B. (1996). DNA strand exchange promoted by RecA K72R. Two reaction phases with different Mg2+ requirements. J. Biol. Chem. *271*, 5712–5724.

Shan, Q., Bork, J.M., Webb, B.L., Inman, R.B., and Cox, M.M. (1997). RecA protein filaments: end-dependent dissociation from ssDNA and stabilization by RecO and RecR proteins. J. Mol. Biol. *265*, 519–540.

Shaner, S.L., and Radding, C.M. (1987). Translocation of Escherichia coli recA protein from a single-stranded tail to contiguous duplex DNA. J. Biol. Chem. *262*, 9211–9219.

Shaner, S.L., Flory, J., and Radding, C.M. (1987). The distribution of Escherichia coli recA protein bound to duplex DNA with single-stranded ends. J. Biol. Chem. *262*, 9220–9230.

Shivashankar, G.V., Feingold, M., Krichevsky, O., and Libchaber, A. (1999). RecA polymerization on double-stranded DNA by using single-molecule manipulation: the role of ATP hydrolysis. Proc. Natl. Acad. Sci. USA *96*, 7916–7921.

Smith, G.R. (2001). Homologous recombination near and far from DNA breaks: alternative roles and contrasting views. Annu. Rev. Genet. *35*, 243–274.

Sommer, S., Boudsocq, F., Devoret, R., and Bailone, A. (1998). Specific RecA amino acid changes affect RecA-UmuD'C interaction. Mol. Microbiol. *28*, 281–291.

Spies, M., and Kowalczykowski, S.C. (2006). The RecA binding locus of RecBCD is a general domain for recruitment of DNA strand exchange proteins. Mol. Cell *21*, 573–580.

Story, R.M., Weber, I.T., and Steitz, T.A. (1992). The structure of the E. coli recA protein monomer and polymer. Nature *355*, 318–325.

Thresher, R.J., Christiansen, G., and Griffith, J.D. (1988). Assembly of presynaptic filaments. Factors affecting the assembly of RecA protein onto single-stranded DNA. J. Mol. Biol. *201*, 101–113.

Tlusty, T., Bar-Ziv, R., and Libchaber, A. (2004). High-fidelity DNA sensing by protein binding fluctuations. Phys. Rev. Lett. *93*, 258103.

Umezu, K., Chi, N.W., and Kolodner, R.D. (1993). Biochemical interaction of the Escherichia coli RecF, RecO, and RecR proteins with RecA protein and single-stranded DNA binding protein. Proc. Natl. Acad. Sci. USA *90*, 3875–3879.

van der Heijden, T., van Noort, J., van Leest, H., Kanaar, R., Wyman, C., Dekker, N.H., and Dekker, C. (2005). Torque-limited RecA polymerization on dsDNA. Nucleic Acids Res. *33*, 2099–2105.

Venkitaraman, A.R. (2004). Tracing the network connecting BRCA and Fanconi anaemia proteins. Nat. Rev. Cancer *4*, 266–276.

Wegner, A. (1982). Treadmilling of actin at physiological salt concentrations. An analysis of the critical concentrations of actin filaments. J. Mol. Biol. *161*, 607–615.

Weiss, S. (1999). Fluorescence spectroscopy of single biomolecules. Science *283*, 1676–1683.

Yang, H., Li, Q., Fan, J., Holloman, W.K., and Pavletich, N.P. (2005). The BRCA2 homologue Brh2 nucleates RAD51 filament formation at a dsDNA-ssDNA junction. Nature *433*, 653–657.

Zhuang, X. (2005). Single-molecule RNA science. Annu. Rev. Biophys. Biomol. Struct. *34*, 399–414.

Zlotnick, A., Mitchell, R.S., Steed, R.K., and Brenner, S.L. (1993). Analysis of two distinct single-stranded DNA binding sites on the recA nucleoprotein filament. J. Biol. Chem. *268*, 22525–22530.